Dissociation of As_4 clusters following valence photoionization and 3*d* core excitation

J. A. Kettunen,[1,*] S. Urpelainen,[1,2] S. Heinäsmäki,[1] and M. Huttula[1]
[1]*Department of Physics, University of Oulu, P.O. Box 3000, FIN-90014 University of Oulu, Finland*
[2]*MAX-IV Laboratory, Lund University, P.O. Box 118, SE-22100 Lund, Sweden*
(Received 14 May 2012; revised manuscript received 29 June 2012; published 3 August 2012)

The VUV-induced photofragmentation of As_4 clusters was studied using photoelectron-photoion-coincidence (PEPICO) spectroscopy. The fragmentation pathways subsequent to outer and inner valence photoionization and resonant photoexcitation were studied by examining the cationic production as a function of electron energy. In addition, regular photoelectron spectroscopy and partial ion yield absorption spectroscopy were employed. In order to enhance the weak signal from the inner valence states, resonant core 3*d* excitation was used in the PEPICO experiment. The fragmentation pathways were inspected with the aid of *ab initio* and thermochemical calculations. The many-electron effects were found to play a major role in the observed inner valence structure and resulting photofragmentation.

DOI: 10.1103/PhysRevA.86.023201 PACS number(s): 36.40.Qv, 36.40.Mr, 32.80.Fb, 33.80.Gj

I. INTRODUCTION

Clusters are an intermediate form of matter, polyatomic particles consisting of a finite number of atoms or molecules. The properties of clusters are studied in order to characterize the evolution of physical features when individual atoms and molecules become larger agglomerations. To form a more comprehensive view of the physical properties of clusters, it is beneficial to investigate the dynamics of both large and small clusters. Especially, properties, such as susceptibility to radiation damage, are important properties when considering nanoscale applications of clusters. In order to be able to create stable functional nanodevices, the dynamics of the fragmentation processes need to be well understood.

Unimolecular photofragmentation of polyatomic particles has been the subject of an immense amount of research (see, for example, Refs. [1–5] and references therein). A traditional approach for inspecting the energy-dependent behavior of multiatomic systems has been the partial ion yield (PIY) technique where the overall production of specific ions is followed as a function of photon energy [6–8]. More detailed information may be gained by combining the detection of two or more of the particles originating from the same quantum-mechanical process. If photoelectron and photoion data are gathered in coincidence, the abbreviation PEPICO is used [9–11].

High-purity arsenic is commonly used as a dopant in the semiconductor industry together with gallium and indium for devices, such as diodes, infrared detectors, and lasers. Nearly all arsenic compounds, especially the inorganic ones, are considerably toxic, and they have been used, among others, as agricultural insecticides. In human populations, arsenic-containing substances have been linked to acute deaths and chronic conditions, such as liver cirrhosis and cancer. Several national and international organizations, such as the World Health Organization and the US Environmental Protection Agency have classified arsenic along with many of its compounds as proven human carcinogens [12,13].

The valence photoelectron spectra (PES) of the group V clusters have been studied extensively. Dyke *et al.* [14] have recorded the He I PES of As_4 and As_2 by heating solid arsenic and copper arsenide; Ebel *et al.* [15] have studied the He I PES of As_2 and As_4 in equilibrium mixtures and As_4 by itself; Wang *et al.* [16] have studied the high-resolution PES of P_4, As_2, and As_4, partially resolving the vibrational structures, in addition to focusing on the Jahn-Teller coupling in the respective ground states [17]. Yoo *et al.* [18] have focused on the partial ion yields of As_{2-4}^+ production from As_4^+ with an emphasis on Rydberg structure, adiabatic ionization and appearance energies, and the thermochemistry up to approximately 20.7 eV of photon energy. Previous papers by Urpelainen and co-workers [19,20] have shed light on the fragmentation pathways, resulting from valence and 4*d* core ionization of Sb_4 clusters.

The ground state $^1A_1$ of the As_4 cluster has tetrahedral symmetry of point group T_d as in the case of antimony and phosphorus tetramers [16,21,22], and the electronic configuration of the As_4 valence may be described using the molecular orbitals (MOs) $(1a_1)^2(1t_2)^6(2a_1)^2(2t_2)^6(1e)^4$ [16]. From here onward, we will refer to the three outermost MOs $2a_1$, $2t_2$, and $1e$ as the outer valence and the two more tightly bound MOs $1a_1$ and $1t_2$ as the inner valence. Zhang and Balasubramanian have performed extensive computations regarding the electronic structure of group V tetramers (P_4, As_4, Sb_4, and Bi_4) [23]. Meier and Peyerimhoff [22] have performed an *ab initio* study on gallium and arsenic compounds and clusters in ionic and neutral forms. For As_4, they have computed the ground-state bond length, stability, and vertical ionization energy for the first three orbitals. Andzelm *et al.* have performed theoretical calculations for As_2 and As_4 molecules, reporting, for example, the vibrational frequencies, equilibrium distances, and ionization energies [24]. As with Sb_4, the inner valence PES of As_4 is not experimentally well known.

In this paper, we report our results on unimolecular VUV photofragmentation of As_4 clusters as a part of our ongoing research on the PES and PEPICO spectroscopy of group V clusters [19,20,25,26]. In the case of Sb_4 clusters, Urpelainen and co-workers [19,25] observed that the inner valence signal was distributed over a wide energy region due to the strong electron correlation of the MOs of mainly atomic 5*s* character. They also found out that the signal from these orbitals was

*antti.kettunen@oulu.fi

greatly enhanced in the resonant Auger process following the $4d \rightarrow 4^{-1}nl$ resonances [where nl denotes a lowest unoccupied molecular orbital-type (LUMO) or a Rydberg-like orbital]. In the present As_4 study, the same effect was exploited. The decay of As_4 was probed by $3d \rightarrow 3d^{-1}nl$ core excitation as it enhanced the production of same final electronic states that can be reached via direct photoionization accompanied by shake-up and correlation satellites.

II. EXPERIMENT

The experiments were performed at MAX-lab (Lund, Sweden) on the gas phase branchline FINEST [27] of the VUV undulator beamline I3 [28]. The PEPICO setup consists of a modified Scienta SES-100 [29,30] hemispherical deflection analyzer (HDA) and a Wiley-McLaren-type [31] time-of-flight mass spectrometer (TOFMS) [32]. The HDA contains a Quantar Model 3394A resistive anode detector, which is used for fast electron detection required by coincidence experiments. The HDA was used for energy-resolved electron detection: A fixed kinetic-energy range was chosen according to the previously studied valence spectrum of As_4 [14–16]. The HDA entrance slit was 0.8 mm (curved), which, together with 100 eV pass energy, provided an approximate analyzer broadening of 400 meV. All electron measurements were performed using the "magic angle" of 54.7° with respect to the electric-field vector of the linearly polarized radiation.

The $3d^{-1}$ ionization energy of solid As has been found to be 42 eV [33], and when corrected by the As work function for polycrystalline solid (3.75 eV [12]), it becomes 45.75 eV with respect to the vacuum level. PIY spectra were recorded between 41 and 50 eV in order to locate the $3d \rightarrow 3d^{-1}nl$ resonances as the binding energy of the As_4 $3d$ electrons was expected to be slightly higher than that of the solid-state As. The PIY data were gathered for As_4^+ and its possible fragments. The PIY intensity was normalized to the photon flux recorded using a Keithley picoammeter connected to an AXUV-100 photodiode. In this process, the known device-dependent quantum efficiency values [34] were taken into account. The photon bandwidth was approximately 54 meV.

The photon energy of $h\nu = 43.65$ eV was used for the coincidence experiment. For PEPICO data acquisition, the TOFMS was used in a pulsed mode so that each ion acquisition was triggered separately either by an actual electron detection or a so-called random trigger from a separate pulse generator. The PEPICO data handling has been elaborated by Kukk *et al.* [30]. In the relative coincident ion yield (CIY) treatment, the error bars have been derived by using the total differential of the expression for relative ion intensities (yields) $I_i^{\mathrm{rel}}(E) = I_i(E)/\Sigma_j I_j(E)$, where $I_i(E)$ is the absolute ion yield for an ion specified by i at energy channel E and $I_j(E)$ runs over all absolute ion yields within the same energy channel. The absolute error for all the ion-specific absolute yields has been taken as $\Delta I_i(E) = 2\sigma(I_i(E)) = 2\sqrt{I_i(E)}$, assuming Poissonian statistics. These errors are taken from the total channel-specific counts including the false ion background.

As_4 vapor was produced from commercial sponges (Strem Chemicals Inc., 99.99% purity) by using a resistively heated oven designed and built at the University of Oulu. During the initial heating, TOF spectra were recorded continuously, and various oxides, such as As_4O_6, were detected. The oxide production subsided after some hours of steady heating at 480 K according to thermocouple readings from within the oven. It was noted that the thermal production of As_4 from pure arsenic was clearly dominant within this temperature range as the literature indicates: In previous papers, the appearance of As and As_2 from a heated solid-state sample required temperatures in the order of 1000–1800 K, whereas, As_4 dominated at temperatures of 400–850 K [14,18]. Valence region As_4 photoelectron spectra were obtained for binding-energy calibration purposes with the inclusion of Kr. The common residual gases (H_2O and N_2) were also used in the energy calibration.

III. CALCULATIONS

Ab initio density-functional theory (DFT) and thermochemical calculations were performed in order to correlate the observed fragmentations with specific fragmentation pathways subsequent to valence photoionization of As_4.

The DFT calculations were performed with the ERKALE code [37]. The computations were performed by using a Gaussian aug-cc-pVTZ basis set [38] for the As atoms. In the density-functional theory, the local-density approximation was used for exchange, and the correlation was taken into account by the Vosko-Wilk-Nusair method [39]. For more details on the computational methodology, see Lehtola *et al.* [40].

The thermochemical calculations are based on previously determined heat of formation $[\Delta_f H^0(As_n)]$ and adiabatic ionization energy $[I_A(As_n)]$ data (see Yoo *et al.* [18] and references therein, notably Refs. [17,35,36]) (see Table I). With the numerical values, we follow the formulation of Refs. [41,42] where the cationic dissociation and appearance energies are derived using the heat of formation changes between the precursor molecules and their fragments. These relative energy differences are then combined with an approximation for the I_A of the As_4 molecule, which is set to the theoretical value of 7.83 eV according to Wang *et al.* [17], yielding a constant shift applied to all calculated appearance energies. In the calculations, $T = 0$ K is assumed, which introduces some inaccuracy with respect to the experiment. The final forms for evaluating the thermochemical appearance energies (E_t) can be formulated by employing the relations for the dissociation

TABLE I. The heats of formation (eV) and adiabatic ionization energies (eV) for As_n used for determining the thermochemical thresholds (obtained from Yoo *et al.* [18] and references therein, notably [17,35,36]).

	$\Delta_f H^0$	I_A
As_4	1.67	7.83
As_3	2.73	7.19
As_2	2.01	9.69
As	2.98	9.7886

energies ($D_{n,p}, D^+_{n,p}$) and I_As [41,42],

$$D_{n,p} = \Delta_f H^0(\mathrm{As}_{n-p}) + \Delta_f H^0(\mathrm{As}_p) - \Delta_f H^0(\mathrm{As}_n), \quad (1)$$

$$D^+_{n,p} = D_{n,p} + I_A(\mathrm{As}_{n-p}) - I_A(\mathrm{As}_n), \quad (2)$$

$$E_t(\mathrm{As}_j{}^+) = D^+ + I_A(\mathrm{As}_4), \quad (3)$$

where I_A is the adiabatic ionization energy, E_t is the thermochemical appearance energy, n is the number of arsenic atoms in the parent, p is the number of arsenic atoms in the fragment, $j = 1,2,3$, and D^+ contains all the involved dissociation energies with the charge taken into account. By adding all the involved heats of formation, one may obtain fragmentation thresholds for cation-producing pathways with multiple dissociations as in the case of the ionized and excited parent molecules,

$$\mathrm{As}_4{}^+ \rightarrow \mathrm{As}_3{}^+ + \mathrm{As} \rightarrow \mathrm{As}_2{}^+ + \mathrm{As} + \mathrm{As}. \quad (4)$$

As noted by Yoo and co-workers, the heat of formation and I_A values for As_{1-4} are likely to contain some inaccuracies [18]. For example, some values are given as upper limits, and thus, the present calculations should be considered as a means to obtain the overall trend with respect to fragmentation pathways opening subsequent to valence photoionization.

IV. RESULTS AND DISCUSSION

A. As_4 $3d \rightarrow 3d^{-1}nl$ partial ion yields

The $3d \rightarrow 3d^{-1}nl$ resonances were found in the energy range of 41–50 eV. The recorded PIY spectra are displayed in Fig. 1. The positions of the largest most evident structures have been tabulated in Table II where the relative intensities of the cations are also shown. The intensities have been determined through the absolute ion counts at the specified positions. Figure 1(a) displays a clear enhancement of all cationic production divided within two major structures labeled A and B. As a starting point, it is assumed that this structure consists of the LUMO excitation from the two separate spin-orbit separated $3d$ corelike orbitals with a vibrational envelope dependent on the Franck-Condon factors. As may seen from Fig. 1, As^+ is the clearly dominating cation. In Fig. 1(b), the overall structure appears to follow a Rydberg-like progression, which converges around $h\nu = 50$ eV. The splitting of the Rydberg-like structures is in the order of 600–800 meV (see Table II). In Fig. 1(b), the production of As^+ is again favored throughout, and the yields of $As_2{}^+$ and $As_3{}^+$ are clearly enhanced at resonant energies below 48 eV up to the structure labeled G.

The spin-orbit splitting in direct photoionization of As $3d^{-1}$ on a Si(111):As 1×1 surface has been reported to be 690 meV with the statistical ratio of 3:2 [43], which is what would be expected in the case of atomiclike core orbitals. For the data of this experiment, least-squares fits [44] of symmetric Voigt peaks were performed for the As_4 fragments of Fig. 1(a). For As^+, the most abundant cation, a split of 680 meV is obtained with an area ratio of 1:2.15. For $As_3{}^+$, a similar split of 700 meV is received with an area ratio of 1:2.05. In turn, the fit for $As_2{}^+$ yields a split of 680 meV with an area ratio of 1:2.10. However, for $As_4{}^+$, in clear contrast to the other cations, the split appears to be 760 meV with an area ratio of 1:3.40. As a general explanation for the overall trend, it may be noted that the absorption cross section is affected by the resonant state properties, and thus, a reasonable assumption may be

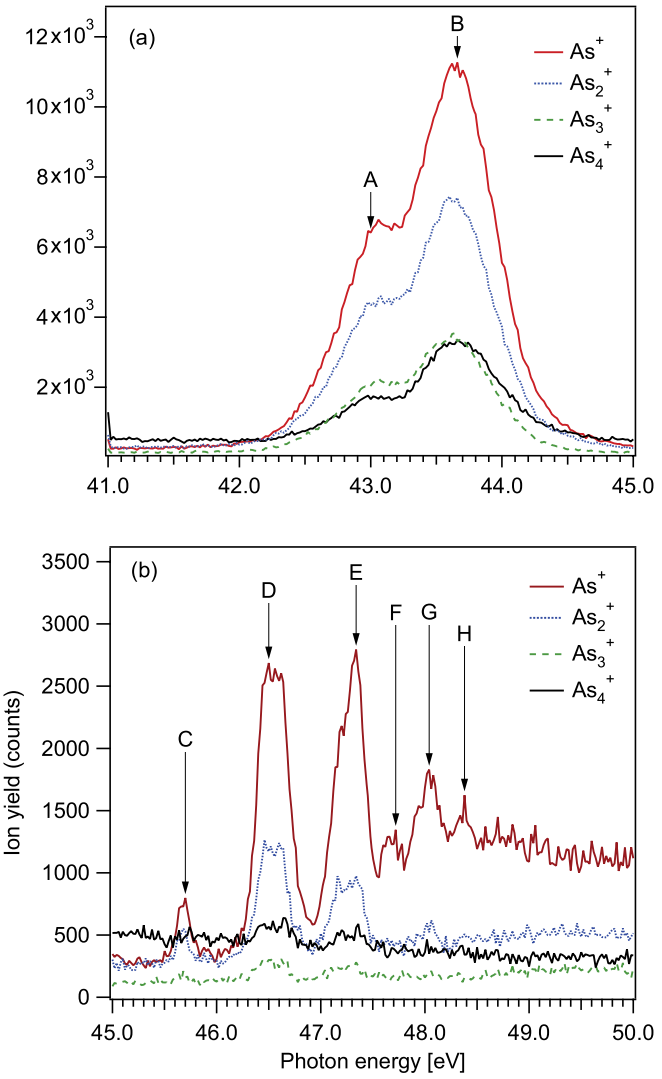

FIG. 1. (Color online) PIYs for $As_n{}^+$ ions between photon energy ranges (a) 41–45 eV and (b) 45–50 eV. The energies for the structures are found in Table II.

TABLE II. The most evident structures observed in PIY spectra at different energies (eV) of Fig. 1 along with the relative intensities (%) of the cations ($As_{1-4}{}^+$).

		Relative intensities			
Label	Energy	As^+	$As_2{}^+$	$As_3{}^+$	$As_4{}^+$
A	42.98	44	30	13	12
B	43.66	44	29	13	13
C	45.70	40	27	8	25
D	46.50	57	25	6	12
E	47.34	61	21	6	12
F	47.72	58	19	8	16
G	48.04	64	18	6	12
H	48.38	62	19	6	13

explored: The LUMO excitations likely consist of a large number of energetically close states, and these states possess different symmetry properties. In addition, the shallow 3*d* corelike orbitals are likely not completely atomic in character but instead, consist of several MOs, such as in the case of Sb_4 clusters [20]. The symmetry properties then determine whether the specific excitations are allowed, and thus, the total intensity ratio between the spin-orbit split components in the absorption spectra does not reflect the initial-state population of the 3*d* corelike orbitals alone.

B. As_4 photoelectron spectrum

The outer valence photoelectron spectrum of As_4 is well known from previous papers [14–16]. A nonresonant PES recorded in our experiments is depicted in Fig. 2 using $h\nu = 25.00$ eV. Mulliken population analysis [16,24] indicates that the three outermost MOs are mainly of As 4*p* character, and the two inner valence MOs are mainly of As 4*s* character. The first two MOs, $1e$ and $2t_2$, being orbitally degenerate, display split structure due to the Jahn-Teller effect, whereas, the $(2a_1)^{-1}$ is known to possess a resolvable vibrational structure containing only a single ν_1 progression. This, however, is not resolved in the spectrum of Fig. 2. The vibrational structures of the $(1e)^{-1}$ and $(2t_2)^{-1}$ bands are also not resolved, but they have been previously concluded to display the ν_2 and ν_3 progressions for the $(1e)^{-1}$ and $(2t_2)^{-1}$ bands, respectively—this has been concluded by the aid of a comparison with the P_4^+ spectrum, which is similar to As_4^+ and Sb_4^+, all being isoelectronic with respect to valence orbitals (see Wang *et al.* [16] and references therein).

The fact that the inner valence MOs have not been clearly visible in the spectra recorded using He I irradiation has been attributed to the low photoionization cross section of these MOs [14]. However, the reason is likely to be more complicated: The electron correlation causes the inner valence electrons to be distributed among numerous electronic states, thus distributing the spectral intensity to a wide energy region. The inner valence MOs largely consist of an As 4*s* contribution [16,24], and it is well known (see, for example, Refs. [19,20,45]) that the outer *s* orbitals exhibit strong electron correlation.

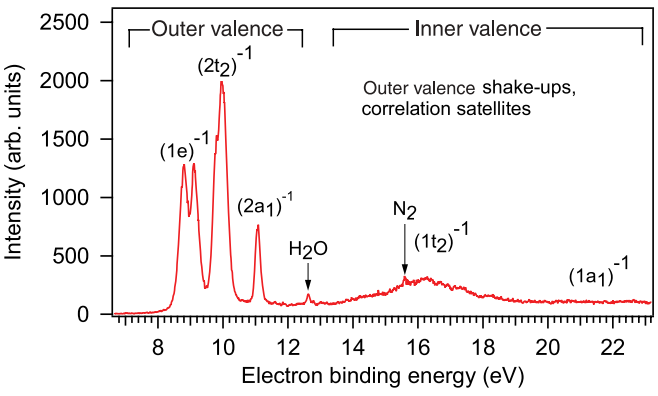

FIG. 2. (Color online) Nonresonant outer and inner valence photoelectron spectrum of As_4. The As_4 photoelectron bands have been identified along with the traces of water and nitrogen. The inner valence bands of $(1t_2)^{-1}$ and $(1a_2)^{-1}$ cannot be clearly recognized in the spectrum, but the labels are placed according to the theoretical predictions. (See text for details.)

The structure between 13.5 and 19.5 eV has not been experimentally identified, but calculated vertical ionization energies (VIEs) for the inner valence MOs $(1t_2)^{-1}$ and $(1a_1)^{-1}$ are placed roughly at 15.8 and 22.3 eV, respectively [22]. In turn, Andzelm and co-workers report the VIEs for inner valence orbitals with two different methods at 17.00 and 15.69 eV for $(1t_2)^{-1}$ and 22.68 and 21.43 eV for $(1a_1)^{-1}$ [24]. For the inner valence MOs, comparison between experimental and theoretical ionization energy is not performed in the existing literature. However, for P_4, Brundle *et al.* [46] and Banna *et al.* [47] have observed the inner valence as a split-structure band with no clear sign of orbital photoelectron bands. Based on all the previous information about the nature of the broadly spread inner valence bands, the observed structure can be tentatively assigned to consist of the correlating $(1t_2)^{-1}$ and $(1a_1)^{-1}$ states possibly in combination with many-electron processes. The degenerate $1t_2$ MO may be further dispersed by the Jahn-Teller effect.

C. As_4 photoelectron-photoion coincidence on resonance

1. Overview

A PEPICO map of As_4 fragmentation using the resonant energy of 43.65 eV (B in Fig. 2) is depicted in Fig. 3. The ion-specific absolute and relative CIYs at the resonant energy are presented in Figs. 4(a) and 4(b). It is worth noting that, for clearer presentation, the relative yields have been presented only for the inner valence region. By comparing the PEPICO map with the PES of Fig. 2, it can be noted that the

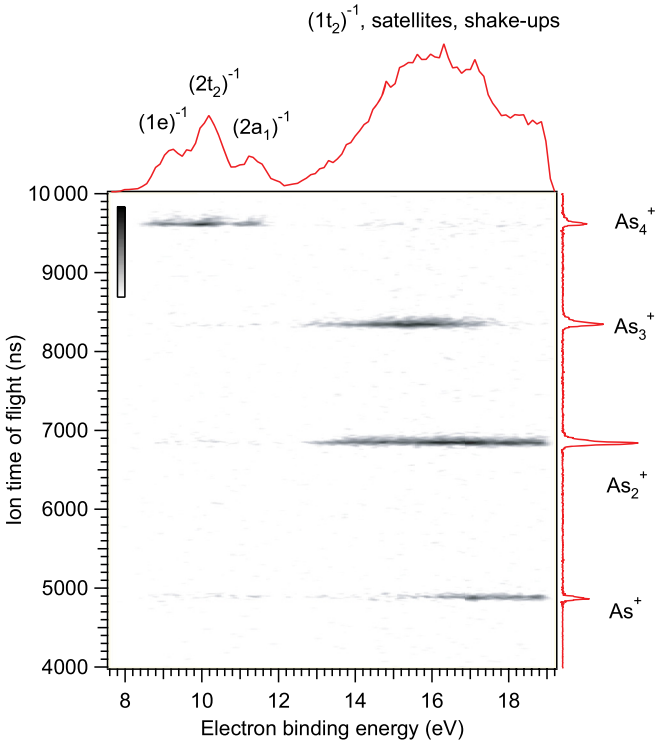

FIG. 3. (Color online) The PEPICO map of the valence region of As_4. The ions and relevant electronic states are identified.

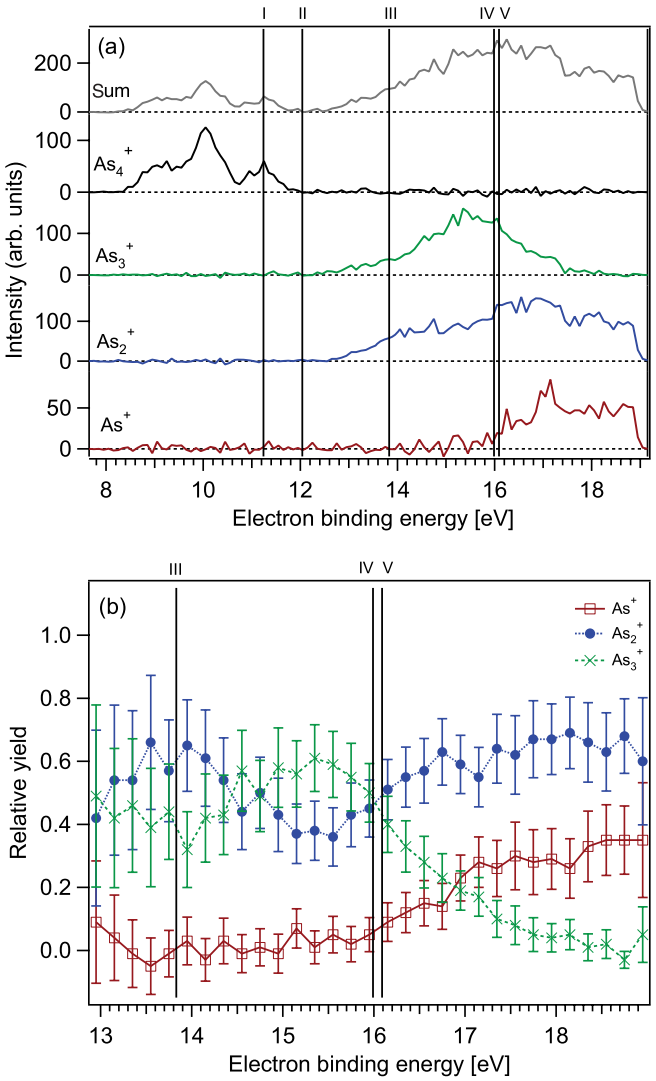

FIG. 4. (Color online) (a) The absolute CIYs for As_4 valence photoionization products and their sum using the resonant energy of 43.65 eV. The intensities are in arbitrary units, and the yields are in absolute scale. The data have been extracted with the step size of 100 meV. (b) The relative CIYs for As_{1-3}^+ over the inner valence energy region. The used step size is 200 meV. The vertical lines refer to the calculated thermochemical appearance energies E_t (see Table III).

inner valence region is radically enhanced with the resonant excitation. The enhancement is to be expected as the excited resonant states are most likely to decay via the spectator Auger process such that the initially excited electron remains as a spectator through the process, thus, increasing the intensity of the excited final states [48]. This decay leads to ionic states of the form $(1t_2)^{-1}(2a_1 2t_2 1e)^{-1}nl$ and $(2a_1 2t_2 1e)^{-2}nl$. The coupling of the two holes and the excited electron leads to a large number of states, which are spread in energy. These states can be further split by the spin-orbit interaction and the Jahn-Teller effect. This process is energetically equivalent to direct photoionization accompanied by a shake-up transition or photoionization of correlation satellite states.

Qualitatively, it can be immediately noticed from Figs. 3, 4(a), and 4(b) that the overall pattern appears to follow an energetically plausible trend. The outer valence photoionization is mostly seen to lead to stable As_4^+ cations with miniscule potential yields of smaller fragments. This is in clear contrast with the inner valence. The observed behavior is similar to the isoelectronic Sb_4 of the same symmetry [19]. Before reaching 16 eV, As^+ begins to appear, which correlates energetically with the theoretically predicted appearance for the $(1t_2)^{-1}$ band [22,24].

The relative yields of Fig. 4(b) display an interesting feature with respect to As_2^+ and As_3^+ production within the energy range of 14.5 and 16.5 eV: The As_3^+ production is seen to experience a sudden increase, whereas, the total coincident ion production also progresses toward its highest observed value. This may indicate the location of a specific electronic state with the assumption that the fragmentation products are state specific. After the crossing observed at 17 eV, the relative production of As_3^+ is seen to decrease noticeably, whereas, the relative yields of As^+ and As_2^+ appear to follow a constant ratio within the error limits, indicating fragmentation channels competing in parallel. The energy region reported for the $(1a_1)^{-1}$ band, around 22 eV [22,24], is not covered by our PEPICO experiment.

2. *Energetics*

The PIY study performed by Yoo and co-workers [18] yields appearance energies of 10.99, 12.096, and 14.85 eV (determined via a yield curve intersection of the base line) for As_3^+, As_2^+, and As^+, respectively, and they report the inferred 0 K E_t's. The energetical trend of the cationic fragment products is also seen in the present experiment. By their energies, the only energetically allowed nonparent cation for the outer valence states should be As_3^+, which is not abundantly detected until the inner valence region is reached. This may be explained by the inherent differences between energy-resolved PEPICO with constant photon energy and photon-energy-scanned PIY experiments, which probe through all the resonant states.

The possible singly charged fragmentation products are listed in Table III along with the *ab initio* and thermochemical energies where the pathways and their associated thresholds are indexed with Roman numerals in increasing order of assumed dissociation energy. The table also includes the experimentally inferred 0 K appearance energies [18] for the cations.

TABLE III. As_4^+ fragmentation products, the *ab initio* dissociation (D_a) and appearance energies (E_a), the thermochemical dissociation (D_t) and appearance energies (E_t), and experimentally inferred cationic 0 K appearance energies (E_e) [18]. All energies are reported in electron volts. The calculated appearance energies assume $I_A(As_4) = 7.83$ eV [17].

	Fragments	D_a	D_t	E_a	E_t	E_e[a]
I	$As_3^+ + As$	2.35	3.41	10.18	11.24	11.23
II	$As_2^+ + As_2$	0.58	4.21	8.41	12.04	12.338
III	$As^+ + As_3$	5.18	6.00	13.01	13.83	15.09
IV	$As_2^+ + 2As$	5.87	8.16	13.70	15.99	
V	$As^+ + As + As_2$	5.94	8.26	13.77	16.09	
VI	$As^+ + 3As$	11.23	9.62	19.06	20.05	

[a]From Yoo *et al.* [18].

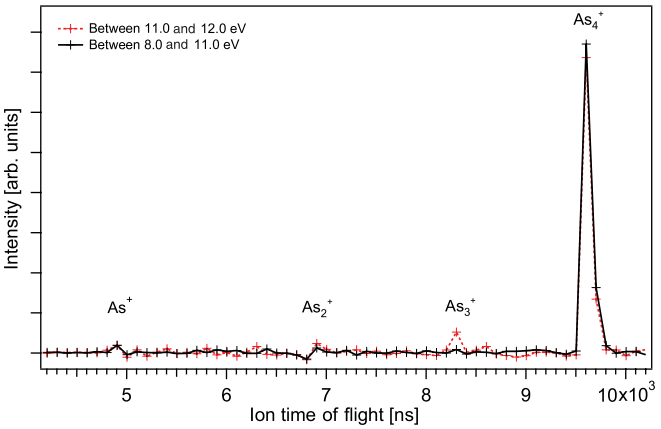

FIG. 5. (Color online) Coincident TOF spectra extracted from the outer valence energy region above and below the $(2a_1)^{-1}$ band (see Figs. 3 and 4). The difference in As_3^+ production between the two energy regions is concluded to occur due to the crossing of the thermochemical threshold I (see Table III).

Threshold I (observed cation being As_3^+) has been seen as the energetically first fragmentation channel [18]. With the present constant photon energy experiment, the outer valence hole states appear mostly nonfragmenting: As may be observed from Fig. 4(a), the previously determined appearance threshold for As_3^+ [18] is crossed at the higher-energy side of the outer valence, yet, only a miniscule activity of As_3^+ production is observed between 11 and 12 eV in the CIYs of Fig. 4. For more careful analysis, coincident TOF spectra have been extracted from the outer valence, containing the cationic production below and above the thermochemical threshold I (see Fig. 5). The TOF spectra indicate that As_3^+ production is indeed detected within the higher-energy end of the outer valence, whereas As^+ and As_2^+ are not detected beyond levels, which are likely results of statistical noise due to random ion background removal.

The inner valence PES structure is observed to begin approximately from 13 eV onward, between 0.5 and 1.0 eV before the expected crossing of threshold II (As_2^+) as determined by the calculated and observed appearance energies. Thus it is energetically expected that the inner valence ionization produces at least As_3^+ and As_2^+. This is seen at the energy region between 13 and 15 eV where As_4^+ activity is considerably small and is assumed to consist of statistical noise on an energetical basis.

Threshold III (As^+), previously 0 K inferred at 15.09 eV [18] from PIY data, is predicted to be crossed before 14 eV on the basis of the heats of formation, however, the yield of As^+ is noted to increase from negligible intensity only after 15 eV.

Thresholds IV (As_2^+) and V (As^+) are expected close to 16 eV. Both IV and V are assumed to cause multiple dissociations,

$$As_4^+ \rightarrow As_2^+ + As_2 \rightarrow As_2^+ + As + As, \qquad (5)$$

$$As_4^+ \rightarrow As_2^+ + As_2 \rightarrow As^+ + As + As_2. \qquad (6)$$

Interestingly, at 14.5–16 eV, the relative yield of As_3^+ is momentarily enhanced. This might indicate As_2^+ being broken into $As^+ + As$, but this is not clearly reflected in the As^+ yield between 15 and 16 eV. The 0 K threshold for V (Table III) is expected to be crossed in this region, so the appearance of this pathway appears energetically plausible. Another possibility is that As_3^+ is created via some direct fragmentation process, over-riding the energetical tendency. On the other hand, the crossing observed at 16 eV clearly indicates the crossing of new thresholds: The As_3^+ yield diminishes toward zero, correlating with the opening of pathways IV and V.

As may be noted from Table III, complete atomization of As_4^+ appears to be unlikely below 20 eV. However, the PIY data of Yoo and co-workers [18] gives an indication of some As^+ production intensification with respect to the larger fragments, which may indeed correlate with the opening of the complete atomization pathway.

Surprisingly, the *ab initio* calculations indicate that the channel for $As_2^+ + As_2$ should open before $As_3^+ + As$, which is not experimentally observed by us or Yoo *et al.* [18]. This suggests a failure of the DFT predictions for thresholds I and II (Table III), however, the other energies are seen to follow the same qualitative trend as the experiment and the thermochemical estimates provide.

V. CONCLUSIONS

In this paper, we have presented an experimental valence PES of As_4^+, PIYs for the $3d \rightarrow 3d^{-1}nl$ resonances between photon energies of 41–50 eV, and energy-resolved valence PEPICO fragmentation data subsequent to resonant $3d$ excitation. The partial ion yields display resonant $3d \rightarrow 3d^{-1}nl$ structures, indicating LUMO and converging Rydberg-like excitations. The PIY data between 41 and 45 eV reveal that the area ratios and observed structure splits are quite similar for As_{1-3}^+, however, the relative ratio and observed split are noticeably different for As_4^+.

Analysis performed on the relative coincident yields indicates some oscillation in the fragment production at the lower-energy inner valence region (13–16 eV). In the region between 14.5 and 16 eV, As_3^+ production is seen to experience a noticeable increase. In the higher energies, after 16 eV, As_3^+ production is seen to steadily decrease toward zero, whereas, the production of As^+ and As_2^+ appears to compete in parallel. All in all, from the following reasoning, it is concluded that the inner valence structure observed approximately between 13 and 19 eV is dominated by states resulting from simultaneous outer valence photoionization and shake-up transitions $(2a_1 2t_2 1e)^{-2}nl$, inner valence photoionization $(1t_2)^{-1}$, and inner valence photoionization combined with shake-ups $(1t_2)^{-1}(2a_1 2t_2 1e)^{-1}nl$. Previously, the apparent weak cross section of the inner valence MOs $1t_2$ and $1a_1$ had been attributed as the reason for the low experimental intensity [14], however, it is reasonable to expect that the high amount of intensity distribution due to configuration interaction and the complex interplay between the Jahn-Teller effect and the spin-orbit splitting plays a major role, especially with $1t_2$.

As mentioned in the paper by Zhang and Balasubramanian [23], the first excited state of As_4 is placed 3.4 eV above the neutral ground state, thus, yielding a first approximation for evaluating the possible shake-up energy shifts for the photoionized valence states coupled with simultaneous shake-ups.

This would then indicate that the outer valence photoionized states $(2a_1 2t_2 1e)^{-1}$, placed roughly between 8 and 12 eV, would be accompanied by simultaneous shake-up states at the region between 12 and 16 eV, not taking into account the relaxation effects subsequent to photoionization. Following this reasoning, the structure observed in the approximate binding-energy region of 12–16 eV is related to $(2a_1 2t_2 1e)^{-2}nl$ outer valence shake-up states where two holes are made on bonding orbitals and one electron resides in a nonbonding or antibonding LUMO or a Rydberg orbital, thus, resulting in stronger fragmentation of the cluster.

When the fragmentation of valence-ionized As_4 (Fig. 4) is approached purely on an energetical basis, a qualitative match between the thermochemical threshold values and the relative CIYs is observed. The DFT calculations yield a lower threshold energy for the first pathway, resulting in As_2^+ production in comparison to the first As_3^+ threshold—this is not verified by the present experiment. The thresholds for multiple dissociations were also considered, and an agreement is noted specifically with the appearance of pronounced As^+ and As_2^+ production after the crossings between 16 and 18 eV of electron-binding energy. The observed dip in relative As_2^+ production between 14.5 and 16 eV may be explained by the increased As^+ production.

The observed enhancement of As_3^+ production at 15.4 eV [Fig. 4(b)] is energetically rather close to the calculated VIEs for the $(1t_2)^{-1}$ state, which have been placed at 15.8 [22], 17.00, and 15.69 eV [24]. This may indicate that the observed enhancement is tied into the appearance of the $(1t_2)^{-1}$ state with some overlap from the outer valence shake-up states. Following the energetical principle of shake-ups and correlation satellites lying in higher energies, the $(1t_2)^{-1}(2a_1 2t_2 1e)^{-1}nl$ states would then be located beyond the energy of 16 eV. With these states, one hole is located on the strongly bonding $1t_2$ orbital, one on the bonding outer valence orbitals, and one electron resides on a nonbonding or antibonding LUMO-Rydberg orbital.

In conclusion, it is necessary to acknowledge the benefits of performing electronic structure studies with coincidence techniques. For example, in the case of highly convoluted electron spectra of clusters where overlaps of many different electronic states are expected to be seen, the PEPICO technique provides a method to attempt the separation of the individually contributing states. This is especially pronounced in cases where the molecular properties may be made manifest by features, such as state-selective fragmentation pathways. As separate techniques, photoelectron and ion mass spectroscopies serve many purposes, but the properly combined result often proves greater than their direct sum.

ACKNOWLEDGMENTS

This work has been financially supported by the Research Council for Natural Sciences and Engineering of the Academy of Finland. The research leading to these results has received funding from the European Community's Seventh Framework Programme (FP7/2007-2013) under Grant Agreement No. 226716. J.A.K. expresses his thanks and acknowledges The Finnish Academy of Science and Letters and the Vilho, Yrjö, and Kalle Väisälä Foundation for supporting this research. S.U. would like to acknowledge the Research Council for Natural Sciences and Engineering of the Academy of Finland and Lund University for financial support. In addition, the authors would like to thank E. Kukk for general support and the original macros used for coincidence data handling. S. Aksela is acknowledged for his contribution to the oven design. The staff at MAX-laboratory is also acknowledged for their assistance during the experiments.

[1] L. J. Butler and D. M. Neumark, J. Phys. Chem. **100**, 12801 (1996).
[2] Y.-P. Lee, Annu. Rev. Phys. Chem. **54**, 215 (2003).
[3] H. Sato, Chem. Rev. **101**, 2687 (2001).
[4] J. H. D. Eland, Laser Chem. **11**, 259 (1991).
[5] R. A. W. Johnstone and B. N. McMaster, Mass Spectrom. **3**, 1 (1975).
[6] M. N. Piancastelli, W. C. Stolte, G. Öhrwall, S.-W. Yu, D. Bull, K. Lantz, A. S. Schlachter, and D. W. Lindle, J. Chem. Phys. **117**, 8264 (2002).
[7] E. Kukk, M. Huttula, J. Rius i Riu, H. Aksela, and S. Aksela, J. Phys. B **37**, 2739 (2004).
[8] W. C. Stolte, R. Guillemin, S.-W. Yu, and D. W. Lindle, J. Phys. B **41**, 145102 (2008).
[9] R. E. Continetti, Ann. Rev. Phys. Chem. **52**, 165 (2001).
[10] C. Miron and P. Morin, Nucl. Instrum. Methods Phys. Res. A **601**, 66 (2009).
[11] T. Baer, Int. J. Mass. Spectrom. **200**, 443 (2000).
[12] W. M. Haynes, *CRC Handbook of Chemistry and Physics*, 91st ed., Internet version edited by D. R. Lide (CRC/Taylor & Francis, Boca Raton, FL, 2012).
[13] S. C. Grund, K. Hanusch, and H. U. Wolf, *Ullman's Encylopedia of Industrial Chemistry* (Wiley-WCH, Weinheim, 2008).
[14] J. M. Dyke, S. Elbel, A. Morris, and J. C. H. Stevens, J. Chem. Soc., Faraday Trans. 2 **82**, 637 (1986).
[15] S. Ebel, H. T. Dieck, and H. Walther, Inorg. Chim. Acta Lett. **53**, L101 (1981).
[16] L.-S. Wang, B. Niu, Y. T. Lee, and D. A. Shirley, Phys. Scr. **41**, 867 (1990).
[17] L.-S. Wang, B. Niu, Y. T. Lee, D. A. Shirley, E. Ghelichkani, and E. R. Grant, J. Chem. Phys. **93**, 6318 (1990).
[18] R. K. Yoo, B. Ruscic, and J. Berkowitz, J. Chem. Phys. **96**, 6696 (1992).
[19] S. Urpelainen, A. Caló, L. Partanen, M. Huttula, J. Niskanen, E. Kukk, S. Aksela, and H. Aksela, Phys. Rev. A **80**, 043201 (2009).
[20] S. Urpelainen, A. Caló, L. Partanen, M. Huttula, S. Aksela, H. Aksela, S. Granroth, and E. Kukk, Phys. Rev. A **79**, 023201 (2009).
[21] M. F. Guest, I. H. Hillier, and V. R. Saunders, J. Chem. Soc., Faraday Trans. 2 **68**, 2070 (1972).
[22] U. Meier and S. D. Peyerimhoff, Chem. Phys. **150**, 331 (1991).

[23] H. Zhang and K. Balasubramanian, J. Chem. Phys. **97**, 3437 (1992).
[24] J. Andzelm, N. Russo, and D. R. Salahub, Chem. Phys. Lett. **142**, 169 (1987).
[25] S. Urpelainen, J. Niskanen, J. A. Kettunen, M. Huttula, and H. Aksela, Phys. Rev. A **83**, 015201 (2011).
[26] M. Huttula, S-M. Huttula, S. Urpelainen, L. Partanen, S. Aksela, and H. Aksela, J. Phys. B **42**, 235002 (2009).
[27] S. Urpelainen, M. Huttula, T. Balasubramanian, R. Sankari, P. Kovala, E. Kukk, E. Nõmmiste, S. Aksela, R. Nyholm, and H. Aksela, AIP Conf. Proc. **1234**, 411 (2010).
[28] T. Balasubramanian, B. N. Jensen, S. Urpelainen, U. Johansson, M. Huttula, R. Sankari, E. Nõmmiste, S. Aksela, H. Aksela, and R. Nyholm, AIP Conf. Proc. **1234**, 661 (2010).
[29] M. Huttula, S. Heinäsmäki, H. Aksela, E. Kukk, and S. Aksela, J. Electron Spectrosc. Relat. Phenom. **156–158**, 270 (2007).
[30] E. Kukk, R. Sankari, M. Huttula, A. Sankari, H. Aksela, and S. Aksela, J. Electron Spectrosc. Relat. Phenom. **155**, 141 (2007).
[31] W. C. Wiley and I. H. McLaren, Rev. Sci. Instrum. **206**, 1150 (1955).
[32] M. Huttula, M. Harkoma, E. Nõmmiste, and S. Aksela, Nucl. Instrum. Methods Phys. Res. A **467**, 1514 (2001).
[33] W. J. Stec, W. E. Morgan, R. G. Albridge, and J. R. van Wazer, Inorg. Chem. **11**, 219 (1972).
[34] [http://www.ird-inc.com].
[35] J. Berkowitz, J. Chem. Phys. **89**, 7065 (1988).
[36] K. S. Bhatia and W. E. Jones, Can. J. Phys. **49**, 1773 (1971).
[37] J. Lehtola, ERKALE HF/DFT from Hel (2012), [http://erkale.googlecode.com].
[38] A. K. Wilson, D. E. Woon, K. A. Peterson, and T. H. Dunning Jr., J. Chem. Phys. **110**, 7667 (1999).
[39] S. H. Vosko, L. Wilk, and M. Nusair, Can. J. Phys. **58**, 1200 (1980).
[40] J. Lehtola, M. Hakala, A. Sakko, and K. Hämäläinen, J. Comp. Chem. **33**, 1572 (2012).
[41] S. G. Lias and J. E. Bartmess, Gas-phase ion thermochemistry, [http://webbook.nist.gov/chemistry/ion/].
[42] K. Kooser, D. T. Ha, E. Itälä, J. Laksman, S. Urpelainen, and E. Kukk, J. Chem. Phys. **137**, 044304 (2012).
[43] R. I. G. Uhrberg, R. D. Bringans, M. A. Olmstead, R. Z. Bachrach, and J. E. Northrup, Phys. Rev. B **35**, 3945 (1987).
[44] E. Kukk, computer code *Spectral analysis by Curve Fitting* (SPANCF).
[45] S. Alitalo, A. Kivimäki, T. Matila, K. Vaarala, H. Aksela, and S. Aksela, J. Electron Spectrosc. Relat. Phenom. **114–116**, 141 (2001).
[46] C. R. Brundle, N. A. Kuebler, M. B. Robin, and H. Basch, Inorg. Chem. **11**, 20 (1972).
[47] M. S. Banna, D. C. Frost, C. A. McDowell, and B. Wallbank, J. Chem. Phys. **66**, 3509 (1977).
[48] H. Aksela, S. Aksela, and N. Kabachnik, *VUV and Soft X-Ray Photoionization*, edited by U. Becker and D. A. Shirley (Plenum, New York, 1996).